

# *SRG*/eROSITA prospects for detection of GRB afterglows

I. Khabibullin<sup>1\*</sup>, S. Sazonov<sup>1</sup> and R. Sunyaev<sup>2,1</sup>

<sup>1</sup>*Space Research Institute, Russian Academy of Sciences, Profsoyuznaya 84/32, 117997 Moscow, Russia*

<sup>2</sup>*Max-Planck-Institut für Astrophysik, Karl-Schwarzschild-Str. 1, 85740 Garching bei München, Germany*

12 October 2018

## ABSTRACT

We discuss the potential of the eROSITA telescope on board the *Spectrum-X-Gamma* observatory to detect gamma-ray burst (GRB) X-ray afterglows during its 4-year all-sky survey. The expected rate of afterglows associated with long-duration GRBs without any information on the bursts proper that can be identified by a characteristic power-law light curve in the eROSITA data is 4–8 events per year. An additional small number,  $\lesssim 2$  per year, of afterglows may be associated with short GRBs, ultra hard (GeV) GRBs and X-ray flashes. eROSITA can thus provide the first unbiased (unaffected by GRB triggering) sample of  $\lesssim 40$  X-ray afterglows, which can be used for statistical studies of GRB afterglows and for constraining the shape of the GRB  $\log N$ – $\log S$  distribution at its low-fluence end. The total number of afterglows detected by eROSITA may be yet higher due to orphan afterglows and failed GRBs. The actual detection rate could thus provide interesting constraints on the properties of relativistic jets associated with collapse of massive stars. Finally, eROSITA can provide accurate ( $\lesssim 30''$ ) coordinates of newly discovered afterglows within a day after the event, early enough for scheduling further follow-up observations.

## 1 INTRODUCTION

The main objective of the *Spectrum-Roentgen-Gamma* (SRG) observatory is to perform a sensitive all-sky survey in the 0.3–12 keV energy band with the eROSITA<sup>1</sup> (Predehl et al. 2011) and ART-XC<sup>2</sup> (Pavlinsky et al. 2011) telescopes. The survey (see §2 for details) will last 4 years and consist of 8 repeated complete scans of the sky. The telescopes will be scanning the sky in great circles as a result of the spacecraft’s rotation with a period of 4 hours around its axis pointed at the Sun. This observational strategy provides the possibility of studying variable and transient X-ray sources on three characteristic time-scales corresponding to 1) the duration of a single scan of a point source,  $\lesssim 40$  s, 2) the duration of a single observation of a source,  $\gtrsim 1$  day (consisting of  $\gtrsim 6$  consecutive rotation cycles, depending on the ecliptic latitude), and 3) the duration of a single all-sky scan (6 months).

Information on temporal behaviour can greatly assist in identifying the types of X-ray sources discovered during the eROSITA all-sky survey. In particular, the X-ray afterglows of cosmic gamma-ray bursts (GRBs) form a class of bright transient sources that usually demonstrate power-law decay during the first hours and days after the burst (see Gehrels, Ramirez-Ruiz, & Fox 2009 for a review). Therefore, GRB afterglows can manifest themselves by a distinct variability pattern on the time-scale of several successive

eROSITA scans, which in principle makes it possible to identify such events by analysing the X-ray light curves of sources detected during the all-sky survey.

The purpose of this paper is to estimate the detection rates of GRB X-ray afterglows during the eROSITA all-sky survey. Previously, Greiner et al. (2000) carried out a search for afterglows of untriggered GRBs in the *ROSAT* all-sky survey (RASS) data and found 23 afterglow candidates. However, a closer examination indicated that at least half and perhaps the majority of these events were flares of late-type stars. Taking into account eROSITA’s better (by a factor of  $\sim 4$  in the 0.5–2 keV energy band) sensitivity and a factor of 2 larger sky coverage (survey duration times field of view area) of the planned survey, we can expect a significantly larger number of detected GRB afterglows. We note in passing that in addition to afterglows, the *SRG* all-sky survey may also detect a significant number of GRBs themselves, depending on the unknown shape of the  $\log N$ – $\log S$  distribution of GRBs at very low fluences. This topic will be addressed elsewhere.

The main motivation for such a study is that eROSITA can provide the *first unbiased sample of X-ray afterglows*. The problem with all existing samples of afterglows is that they are based on triggered GRBs and thus determined by the energy range, sensitivity and strategy of the particular GRB experiments. As we discuss in this paper, eROSITA may find a significant number of afterglows associated with GRBs falling near or below the detection threshold and/or having the spectral maximum outside the energy range of existing GRB monitors. This will make it possible to con-

<sup>1</sup> Extended ROentgen Survey with an Imaging Telescope Array

<sup>2</sup> Astronomical Roentgen Telescope – X-ray Concentrator

struct an unbiased distribution of X-ray afterglow fluxes and will also provide valuable constraints on the shape of the GRB  $\log N$ - $\log S$  distribution at low prompt emission fluences. In addition, eROSITA may find a significant number of 'orphan' afterglows, i.e. events without preceding prompt high-energy emission (e.g. Rossi, Lazzati & Rees 2002; Nakar & Piran 2003), and afterglows associated with 'failed GRBs' (e.g. Huang, Dai & Lu 2002), which will provide interesting constraints on the properties of relativistic jets produced during the collapse of massive stars (MacFadyen & Woosley 1999).

## 2 TASKS AND ANALYTICAL ESTIMATES

The *SRG* observatory will be launched into the L2 point of the Earth-Sun system and the first 4 years of the mission will be devoted to performing an all-sky X-ray survey. The satellite will be rotating with a period of  $T = 4$  hours around its axis pointed at the Sun (or a few degrees away from the Sun, the exact strategy is still to be decided), with the telescopes observing the sky at right angles to the axis. Consequently, the rotation axis will be moving at a speed of 1 deg per day following the orbit of the L2 point around the Sun. As a result, a complete survey of the sky will be done every 6 months and a total of 8 scans will be completed over the course of the mission. With the 1 deg-diameter field of view (FoV), eROSITA will be scanning the sky with a speed  $\frac{dS}{dt} \approx \frac{S_0}{180T} \approx 1 \text{ deg}^2$  per minute (where  $S_0$  is the all-sky area). A typical position on the sky will pass through the FoV during 6 consecutive spacecraft rotations once during each all-sky scan. A single scan of a point source will last  $\simeq 40$  s, the time it takes for the source to cross the FoV through its centre. Therefore, most of the sky will receive an exposure  $\sim 2$  ks by the end of the survey. In reality, the received exposure gradually increases towards the ecliptic poles, so that the ecliptic caps will receive up to  $\sim 30$  ks by the end of the survey (Pavlinisky et al. 2012). This also means that any sources located in these regions will transit the eROSITA FoV during more than 6 successive rotation cycles.

Below we consider two scientifically interesting tasks for the *SRG*/eROSITA survey: i) identification of afterglows without any information about the bursts proper and ii) search for afterglows of triggered (by instruments aboard *SRG* or other observatories) GRBs.

### 2.1 Task 1: identification of afterglows of non-triggered GRBs

*Swift*/XRT observations (Nousek et al. 2006; Zhang et al. 2006) have demonstrated that the light curves of GRB X-ray afterglows cannot always be described by a power law and frequently not even by a combination of several power laws (usually this is the case when one or more flares are observed), as had been previously suggested by *BeppoSAX* observations of late-time afterglows (de Pasquale et al. 2006). However, eROSITA should be most efficient for studying GRB afterglows during the period from  $\sim 10^3$  to  $\sim 10^5$  s after the prompt emission, which usually corresponds to the phase of smooth decay with a slope of approximately 1.2 (see segment III in the cartoon in Zhang et al. 2006). We thus

base our treatment below on the requirement that GRB X-ray afterglow candidates have power-law-like light curves.

Consider the light curve of a GRB afterglow in the 0.5–2 keV energy band (where eROSITA is most sensitive) of the form

$$F_X(t) = F_{X,12} \left( \frac{t-t_0}{12 \text{ hr}} \right)^{-\delta} = F_{X,12} \left( \frac{\tau}{12 \text{ hr}} \right)^{-\delta}, \quad (1)$$

where  $F_{X,12}$  is the X-ray flux at 12 hours after the prompt emission and  $\tau = t - t_0$  is the 'age' of the afterglow, i.e. the time since its onset (in hours). Such an afterglow can be detected by eROSITA until the time

$$\tau_e(F_{X,12}, \delta) = 12 \text{ hr} \left( \frac{F_{X,12}}{F_e} \right)^{1/\delta}, \quad (2)$$

where  $F_e$  is the eROSITA detection limit for one ( $\simeq 40$  s long) scan of a point source. If  $\tau_e \geq nT$ , a light curve containing up to  $n+1$  points can be obtained under suitable spacecraft orientation conditions. In principle, three consecutive flux measurements,  $f_1$ ,  $f_2$  and  $f_3$ , are sufficient to reconstruct a power-law-shaped light curve (see Fig. 1). Indeed, in this case we have three equations for determining three parameters:  $F_{X,12}$ ,  $\delta$  and  $t_0$ , or equivalently,  $F_{X,12}$ ,  $\delta$  and  $\tau_1$ , where  $\tau_1$  is the age of the afterglow during the first successful scan. Specifically, the decay index  $\delta$  can be found by solving the equation

$$2 \left( \frac{f_1}{f_2} \right)^{1/\delta} - \left( \frac{f_1}{f_3} \right)^{1/\delta} = 1, \quad (3)$$

making further determination of  $\tau_1$  and  $F_{X,12}$  trivial. However, in reality  $f_1$ ,  $f_2$  and  $f_3$  are the *measured* values of the afterglow flux, and it is also necessary to take into account the uncertainties associated with flux measurement.

We thus propose as the criteria for identification of afterglow candidates that:

1. There is a sequence of 3 successive scans with the measured fluxes ( $f_1$ ,  $f_2$  and  $f_3$ ) exceeding  $F_e$ ;
2. The  $f_1$ ,  $f_2$  and  $f_3$  fluxes are consistent within their uncertainties with a power-law decay with  $0.5 < \delta < 3.5$  (see Appendix 1);
3. The fluxes measured in scans preceding the  $f_1$  measurement, if there are any, are consistent with zero (to ensure that there is no rising phase that would contradict a GRB afterglow origin);
4. The fluxes (or upper limits) measured in scans succeeding the  $f_3$  measurement, if there are any, confirm the power-law decay.

The second of the conditions listed above, together with the characteristics of eROSITA telescope, implies (see Appendix 1) that the effective limit ( $F_e$ ) for detection and identification of GRB afterglows lies between  $2 \times 10^{-13}$  and  $3 \times 10^{-13} \text{ erg s}^{-1} \text{ cm}^{-2}$  (0.5–2 keV). Here, the higher value is more conservative, as it allows for the possibility of a significant background contribution to the detected photon flux and some uncertainty in the characteristics of the eROSITA telescope; we will use both values for our estimates.

Thus, for confident identification of a candidate afterglow we need at least three consecutive detections above the threshold specified above. This suggests that only afterglows with  $\tau_e \geq 2T = 8 \text{ hr}$  are useful for our purposes. Furthermore, such afterglows can only be suitable if detected for

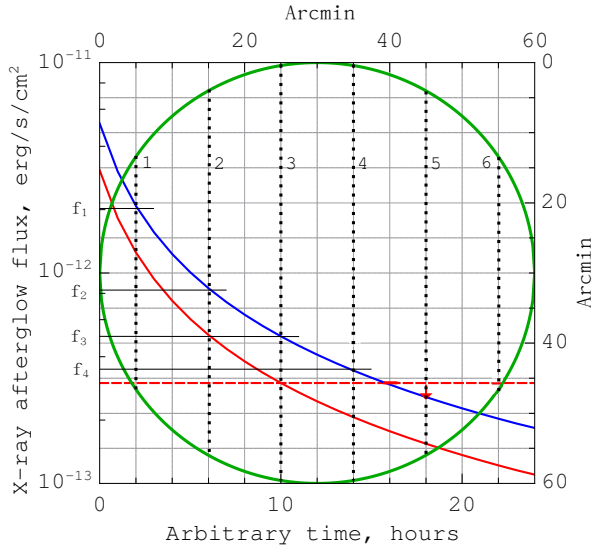


**Figure 1.** Illustration of a typical GRB X-ray afterglow observation by eROSITA. Here, the GRB source passes through the eROSITA FoV (1 deg-diameter green circle with the corresponding right and top axes) during 6 consecutive scans, these transits being shown by vertical black lines. As a result, the afterglow light curve (blue line) is measured at 6 instants separated by 4 hours (see the corresponding left and bottom axes), but only the first 4 measurements exceed the detection limit (horizontal red line).

the first time within  $\tau_m = \tau_e - 2T \geq 0$  after the onset of the afterglow. In other words,  $\tau_m$  defines the ‘time depth’ of an interesting afterglow. For a given afterglow, we can further introduce a survey volume  $d\epsilon = \tau_m dS$ , where  $dS$  is the survey area, and a survey rate  $\frac{d\epsilon}{dt} = \tau_m \frac{dS}{dt}$ . As was mentioned above, the eROSITA scanning speed  $\frac{dS}{dt} = \frac{S_0}{180T}$ . However, because eROSITA will scan a given position in the sky typically for a total of 6 consecutive rotation cycles, only half of the FoV (see Fig. 1) is actually suitable for producing the first point of an at least three-point light curve. Furthermore, only 1/3 of this area has the full time depth  $\tau_m^1$ . For the remaining two thirds, the time depth equals  $\min(T, \tau_m)$ , because a given event could already be detected in the FoV  $T = 4$  hr before. Thus, effectively

$$\frac{d\epsilon}{dt}(\tau_m) = \tau_m \frac{1}{3} \cdot \frac{1}{2} \frac{S_0}{180T} + \min(T, \tau_m) \frac{2}{3} \cdot \frac{1}{2} \frac{S_0}{180T}. \quad (4)$$

Let  $r(\tau_m)$  be the probability density function of  $\tau_m$  for GRB afterglows, normalised to some total GRB rate per unit solid angle,  $R = \int r(\tau_m) d\tau_m$ . Then, the expected number of GRB afterglows detected (and identified as such) by eROSITA during a unit time interval is

$$N_1 = R \left\langle \frac{d\epsilon}{dt} \right\rangle, \quad (5)$$

where

$$\left\langle \frac{d\epsilon}{dt} \right\rangle = \frac{1}{R} \int r(\tau_m) \frac{d\epsilon}{dt}(\tau_m) d\tau_m. \quad (6)$$

<sup>1</sup> Strictly speaking, the time depth of this area is  $\min(T_0, \tau_m)$ , where  $T_0 \approx 180 \times 24$  hr – the eROSITA all-sky scan period, but because the rate of GRBs with  $\tau_m > T_0$  is extremely small, the associated error is negligible.

Therefore, to estimate the expected number of GRB afterglows, one needs to specify the function  $r(\tau_m)$ , which can in principle be derived from observed distributions of GRB fluences, afterglow X-ray fluxes and decay indices.

Before proceeding to accurate estimates, it is useful to make some simplifying assumptions and determine a lower limit for the expected number of GRB afterglows analytically. Due to the form of equation (4), it is natural to divide all potentially interesting afterglows into three categories:

1.  $\tau_e < 8$  hr, hence  $\tau_m = 0$  and  $\frac{d\epsilon}{dt} = 0$ ,
2.  $8 \text{ hr} \leq \tau_e < 12$  hr, hence  $0 \leq \tau_m < 4$  hr and  $\frac{d\epsilon}{dt} = \tau_m \frac{S_0}{360T}$ ,
3.  $\tau_e \geq 12$  hr, hence  $\tau_m \geq 4$  hr and  $\frac{d\epsilon}{dt} = \frac{\tau_m + 2T}{3} \frac{S_0}{360T} = \frac{\tau_e}{3} \frac{S_0}{360T}$ .

The *Swift*/XRT sample of GRB afterglows is consistent with a lognormal distribution of  $F_{X,12}$  (2–10 keV) with  $\langle F_{X,12} \rangle \approx 3 \times 10^{-13} \text{ erg s}^{-1} \text{ cm}^{-2}$  and  $\sigma = 0.5$  (Berger et al. 2005). Assuming a Crab-like X-ray spectrum with a photon index  $\Gamma = 2$  and fixing the light curve slope at  $\delta = 1.3$ , we find that for  $F_e = 3 \times 10^{-13} \text{ erg s}^{-1} \text{ cm}^{-2}$  (0.5–2 keV), approximately half of all *Swift*/XRT GRB afterglows have  $\tau_e \geq 12$  hr and thus fall into the third category described above. Taking into account only such (bright) events, the total rate of afterglows detected by eROSITA will be  $N_1 > \frac{R}{2} \frac{\langle \tau_e \rangle}{3 \cdot 360T}$ , where  $\langle \tau_e \rangle = 12 \text{ hr} \frac{\langle F_{X,12}^{1/\delta} \rangle}{F_e^{1/\delta}}$  is the average over the lognormal distribution of fluxes for  $F_{X,12}$  (0.5–2 keV)  $> F_e$ . Given that  $T = 4$  hr and assuming a total rate of GRBs  $R \approx 1000/S_0$  per year (which corresponds to the *Swift* detection rate recalculated to the full-sky area Dai 2009), we obtain that

$$N_1 > 3.4 \text{ per year}. \quad (7)$$

This is a conservative lower limit on the total afterglow detection rate by eROSITA. In reality, the detection rate should be higher owing to the contribution of weaker afterglows ( $F_{X,12} < F_e$ ), but the result should be sensitive to the shape of the  $\log N$ – $\log S$  distribution of GRB fluences. We obtain more accurate estimates in §3 using Monte Carlo simulations.

## 2.2 Task 2: afterglows of triggered GRBs

A different situation arises if a GRB monitor provides sufficiently accurate coordinates of a GRB. In this case, just one detection will be sufficient to identify its X-ray afterglow and measure its flux at a known time after the prompt emission. The effective eROSITA detection limit for this task is  $F_d = 1 \times 10^{-13} \text{ erg s}^{-1} \text{ cm}^{-2}$  (see Appendix 2), i.e. somewhat lower than for Task 1 discussed above.

In the considered case,  $\tau_m = \tau_e$  and the whole FoV is suitable for the first (and the only needed) detection of an afterglow: 1/6 of the FoV has time depth  $\tau_e$  and the other 5/6 of the FoV  $\min(T, \tau_e)$ . Consequently,

$$\frac{d\epsilon}{dt}(\tau_m) = \tau_e \frac{1}{6} \cdot \frac{S_0}{180T} + \min(T, \tau_e) \frac{5}{6} \cdot \frac{S_0}{180T}. \quad (8)$$

Similar to Task 1, we can find a lower limit on the eROSITA afterglow detection rate for Task 2 using information on *Swift* X-ray afterglows:

$$N_2 > 15 \text{ per year}. \quad (9)$$

This estimate is based on the optimistic assumption that at the time of the *SRG* mission there is a GRB monitor or collection of GRB monitors that constantly cover the whole sky with sufficient sensitivity (corresponding to  $\sim 10^{-8} \text{ erg s}^{-1} \text{ cm}^{-2}$  in 15–150 keV energy band) and localization accuracy ( $\sim 10$  arcmin). For example, *Swift*/BAT provides such characteristics except that its sky coverage is only 1.4 sr (half-coded).

Finally, we note the interesting possibility of searching with eROSITA for afterglows of GRBs detected by the Interplanetary Network (IPN, Hurley et al. 2011). IPN events are often localised (by triangulation) to a large annulus on the sky. The presence of a decaying X-ray source at the intersection of the eROSITA FOV with such an annulus within the first hours–days after a GRB would indicate the detection of an afterglow.

### 3 MONTE CARLO SIMULATIONS: AFTERGLOWS OF LONG GRBS

As was described in §2, the *SRG* all-sky survey will not be homogeneous: the total accumulated exposure (per source) will be significantly larger at high ecliptic latitudes relative to the ecliptic plane. The ecliptic caps will also be advantageous for studying X-ray transients, because a point source will pass through the eROSITA FoV during more than 6 consecutive rotation cycles and can thus be monitored for significantly longer than 1 day. We performed Monte Carlo simulations of the ‘GRB X-ray afterglow sky’ as would be seen by eROSITA, taking the planned survey strategy into account. The simulation consisted of the following steps: 1) model the position of the eROSITA FoV as a function of time (by calculating the phases of rotation around the Sun and the satellite’s axis) over the duration of the survey (several years), 2) assume a total rate, flux distribution and light curve characteristics of afterglows, 3) use these parameters to draw afterglows in random celestial positions, 4) check if a given event falls into the eROSITA FoV and satisfies the detection criteria for Task 1 or Task 2 specified above.

In what follows, we concentrate on classical long ( $> 1$  s) GRBs. Possible additional contributions of other classes of bursts are considered in §5.

#### 3.1 Population of afterglows

The most important and non-trivial part of the simulation is the definition of the intrinsic characteristics of the afterglow population. The problem here is that all samples of afterglows reported in the literature are probably biased relative to the true population of such events, because they are based on samples of GRBs triggered above certain detection thresholds. In fact, the eROSITA all-sky survey might help reveal the intrinsic properties of the GRB afterglow population.

##### 3.1.1 Distribution of GRB prompt emission fluences

The largest existing GRB sample has been provided by the Burst and Transient Source Experiment (BATSE) on board the *Compton Gamma Ray Observatory* (CGRO) (Stern et al. 2001). The  $\log N$ – $\log P$  (here  $P$  is the peak

photon flux in the 50–300 keV energy band) distribution of long bursts from this sample, corrected for the survey’s efficiency function, can be described by a number of models (Stern, Tikhomirova & Svensson 2002, hereafter S02). In our simulations, we used simple approximations to some of these models (namely to SF1,M and SF3,M from Table 2 in S02) and their extrapolations to lower fluences. Specifically, our ‘minimal’ model M1 reproduces the measured  $\log N$ – $\log P$  distribution of bursts above the BATSE detection limit and has a sharp cut-off below this threshold; this model has nearly the same normalisation (total GRB rate) as the SF1,M model in S02. Our ‘medium’ model M2 is the same as M1 but extrapolated by a constant level to lower fluences (down to  $10^{-8} \text{ erg cm}^{-2}$ ); it has nearly the same normalisation as the SF3,M model in S02 and corresponds to increasing star formation at large ( $z > 2$ ) redshifts (see Porciani & Madau 2001). Finally, our ‘maximal’ model M3 is the same as M2 but has an additional power-law component with a slope of 3/2 (also extending down to  $10^{-8} \text{ erg cm}^{-2}$ ), whose normalisation is chosen so as to distort the observed BATSE distribution near its threshold by  $\sim 20\%$ , just within the uncertainty of this distribution (see e.g. Sazonov, Lutovinov & Sunyaev 2004). Such an additional component may be present due to the existence of low-luminosity GRBs (e.g. Kulkarni et al. 1998; Soderberg et al. 2004). Although only a few such events have been detected and associated with nearby ( $z \lesssim 0.1$ ) supernovae so far, the total rate of low-luminosity GRBs in the Universe can be much higher than that of classical (high-luminosity) GRBs (Pian et al. 2006; Liang et al. 2007) and such events occurring at moderate distances ( $z \lesssim 1$ ) can emerge in large numbers at currently inaccessible low fluences.

To proceed to the statistical properties of GRB afterglows, we need to convert the BATSE distribution ( $\log N$ – $\log P$ ) of GRB peak fluxes in the 50–300 keV energy band to a distribution of GRB fluences in the *Swift*/BAT energy band (15–150 keV). To this end, we first convert peak photon fluxes from 50–300 keV to 15–150 keV by the method described in Dai (2009), which provides rather good agreement between the BATSE and BAT  $\log N$ – $\log P$  distributions, and then the 15–150 keV peak photon fluxes to 15–150 keV fluences  $S_{15-150}$  using the average ratio of these two quantities found for the BAT sample (Sakamoto et al. 2011). Fig. 2 shows the resulting distributions (hereafter  $\log N$ – $\log S$ ) for the different GRB population models described above.

##### 3.1.2 Distribution of GRB afterglow fluxes

Comprehensive studies of GRB X-ray afterglows have been done with BeppoSAX (de Pasquale et al. 2006) and *Swift*/XRT (Sakamoto et al. 2008; Gehrels et al. 2008). Due to the higher sensitivity of the latter, Berger et al. (2005) argued that the *Swift*/XRT sample has the least bias, hence we base our analysis on the properties of this sample.

We need to make a conversion from the distribution of GRB prompt emission fluences ( $S$ ) discussed above to a distribution of X-ray afterglow fluxes (e.g. at 12 hours after the prompt emission,  $F_{X,12}$ ). A strong linear correlation was found between  $S$  and  $F_{X,12}$  for *Swift*/XRT GRBs (Sakamoto et al. 2008; Gehrels et al. 2008). We thus use this correlation to predict  $F_{X,12}$  for a given  $S$  but also take into

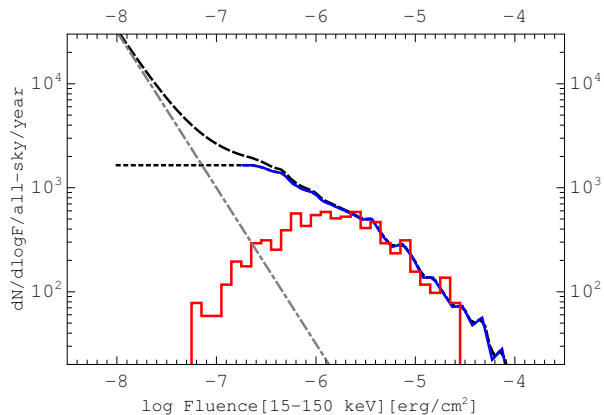


**Figure 2.** GRB number–fluence (15–150 keV) distribution. Blue – the measured distribution of *CGRO*/BATSE bursts, corrected for the detection efficiency function (Stern et al. 2001) and converted from peak fluxes to fluences (see text). Black – various plausible extrapolations of the BATSE distribution to lower fluences: dotted line – flat extrapolation, dashed line – flat extrapolation plus an additional power-law component with a slope of 3/2 (also shown separately by the gray dash-dotted line). Also shown is the observed (and thus distorted at low fluences by the detection efficiency function) distribution of *Swift*/BAT bursts (red).

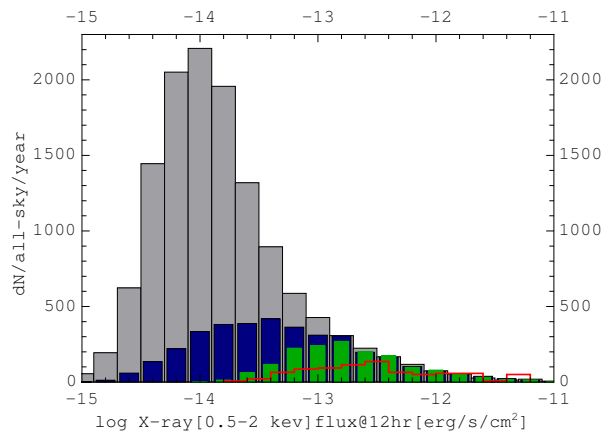


**Figure 3.** Distribution of X-ray afterglow fluxes: red – measured by *Swift*/BAT, green – simulated for model M1 (cut-off at low fluences), blue – simulated for model M2 (flat extrapolation to low fluences), gray – simulated for model M3 (flat extrapolation and additional power-law component with a slope of 3/2 at low fluences). The decrease at the low-flux end in the simulated distributions is due to the truncation of the original GRB samples at  $10^{-8}$  erg  $\text{cm}^{-2}$ .

account the scatter associated with the correlation. Specifically, we distribute  $F_{X,12}$  lognormally with variance  $\sigma = 0.31$  around the expected value. In addition, we make a correction to the 0.5–2 keV energy band from the *Swift*/XRT 0.3–10 keV band) assuming a power-law spectrum with  $\Gamma = 2$  and low X-ray absorbing column density  $N_{\text{H}} \leq 10^{22}$   $\text{cm}^{-2}$ , as is typical of GRB afterglows (Campana et al. 2011). Fig. 3 shows the resulting distributions of afterglow fluxes for the M1, M2 and M3 models described above.

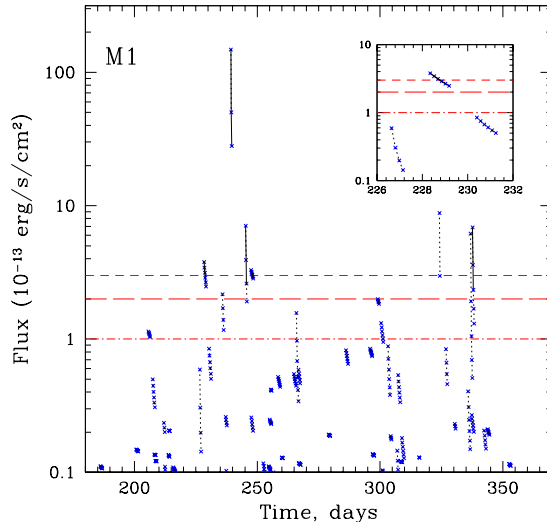


**Figure 4.** Simulated eROSITA half-a-year record history of GRB afterglows for the M1 (minimal) model of GRB population. The red lines indicate different eROSITA detection limits (see text) per scan. Successive detections of the same afterglow are connected with dotted lines. Those light curves that satisfy the identification criteria (at least three flux measurements higher than  $F_e = 2 \times 10^{-13}$  erg  $\text{s}^{-1}$   $\text{cm}^{-2}$ ) are shown by solid lines. The inset shows a few afterglows with better time resolution.

### 3.1.3 Afterglow light curves

To finally simulate the ‘eROSITA afterglow sky’, we need to specify the shape of afterglow light curves. Measured afterglow decay indices are distributed in a narrow range around  $\delta = 1.3$  (Berger et al. 2005), hence we simply fix the light curve slope at this value.

## 3.2 Results

Fig. 4 demonstrates an example of a simulated eROSITA half-a-year all-sky scan for model M1. Table 1 summarises the detection rates for Task 1 and Task 2 for the different considered models, obtained by averaging over a large number of simulated all-sky scans.

The simulated rates are somewhat higher than the analytical lower limits presented in §2 due to i) the contribution of weak ( $F_{X,12} < F_e$ ) events neglected in the analytical calculation (only relevant for the  $N_1$  rate, see §2) and ii) the increased number of scans at high ecliptic latitudes. The differences in the rates obtained for various models (M1, M2 and M3) are associated with the contribution of low-fluence GRBs. The  $N_2$  rate is especially sensitive to such events, because eROSITA with its effective detection threshold ( $F_d$ ) may find a large number of afterglows from weak GRBs that are below the detection threshold of the current and previously flown GRB detectors.

**Table 1.** Summary of the results of simulations for afterglows of long GRBs. Only GRBs with fluence higher than  $10^{-8}$  erg cm $^{-2}$  (15–150 keV) were taken into account. For  $N_1$ , column *a* is for the detection limit  $F_e = 3 \times 10^{-13}$  erg s $^{-1}$  cm $^{-2}$ , while column *b* is for  $F_e = 2 \times 10^{-13}$  erg s $^{-1}$  cm $^{-2}$ . The detection limit for  $N_2$  is  $F_d = 1 \times 10^{-13}$  erg s $^{-1}$  cm $^{-2}$ .

Model	Normalisation, all-sky per year	$N_1$ , per year a	$N_1$ , per year b	$N_2$ , per year
M1	1600	4.4	6.8	19.5
M2	3600	4.8	7.2	27.4
M3	3600+9100	5.0	7.6	55.6

#### 4 CONFUSION WITH OTHER TYPES OF X-RAY SOURCES

Our proposed algorithm for detection of afterglows of non-triggered GRBs (Task 1) is based on checking if three successive X-ray flux measurements separated by 4 hours are consistent with a power-law decline. However, other types of astrophysical objects detected during the *SRG*/eROSITA all-sky survey might also exhibit similar variability properties and could thus be misidentified as GRB afterglows. Below we discuss the most important potential contaminants and how they can be distinguished from afterglows.

##### 4.1 Active Galactic Nuclei

A few millions of active galactic nuclei (AGN) are expected to be discovered by eROSITA all over the sky during the 4-year survey (e.g. Predehl et al. 2011). Although less than  $\sim 10^5$  of these will be brighter than  $F_e = 2 \times 10^{-13}$  erg s $^{-1}$  cm $^{-2}$  (0.5–2 keV) – our effective detection limit for GRB afterglows, it is still an enormous number of sources, some of which may be confused with GRB afterglows. Indeed, AGN are known to be significantly variable on various time-scales from minutes to years (see McHardy 2010 for a review) and usually have Crab-like X-ray spectra with  $\Gamma \sim 2$ , similar to the spectra of GRB afterglows.

The problem of AGN X-ray variability is far from being completely explored and will be one of the key scientific topics of the *SRG* mission. Nevertheless, the results of previous studies allow us to roughly estimate the number of AGN that might resemble GRB afterglows in the eROSITA survey. *Rossi X-ray Timing Explorer (RXTE)* observations have demonstrated that variability properties of AGN are similar to those of Galactic black-hole X-ray binaries (BHB), except that the characteristic time-scales are longer in proportion to the black hole mass (McHardy et al. 2004). Typically, X-ray light curves of AGN are characterised by a power spectrum density (PSD) that can be fitted by a power law with a slope of  $-2$  at high frequencies and a slope of  $-1$  below some frequency  $\nu_B$ . This characteristic frequency correlates with the black hole mass  $M_{BH}$  and accretion rate  $\dot{m}_E$  (in units of the Eddington critical rate) (McHardy 2010) and thus varies significantly between different AGN. Assuming a break frequency  $\nu_B = 10^{-4}$  Hz and rms/flux ratio of 0.2 (typical values for AGN, see McHardy 2010 and references therein), we simulated a large number of AGN light curves using the method described by Timmer & Koenig

(1995) and then applied our GRB afterglow detection criterion (Task 1) to these light curves. We found that the probability for an AGN light curve to have three successive eROSITA flux measurements (separated by 4 hours) that are consistent with a power-law decay with  $0.5 < \delta < 3.5$  is  $\sim 1\%$ . However, in approximately 3/4 of such sequences, the subsequent (fourth) flux will be higher than the third one, which will clearly indicate against a GRB afterglow.

Therefore, the absolute majority of episodes of significant variability in AGN will not resemble GRB afterglows in eROSITA observations. Nevertheless, we can expect a total of a few hundred episodes associated with AGN that will mimic GRB afterglows. Fortunately, most of such bright,  $F_X > F_e = (2 - 3) \times 10^{-13}$  erg s $^{-1}$  cm $^{-2}$  (0.5–2 keV), AGN will manifest themselves as persistent sources (and hence exclude an afterglow origin) over the course of the mission, as they will be repeatedly detected in successive (every 6 months) eROSITA all-sky scans (the detection limit for a point source in one all-sky scan is  $\sim 7 \times 10^{-14}$  erg s $^{-1}$  cm $^{-2}$ , 0.5–2 keV, see Appendix 2). Most of such AGN will also be identified as such through multi-wavelength follow-up efforts (see §4.3 below).

##### 4.2 Stellar flares

Coronally active stars are another population of variable sources that could produce afterglow-like light curves. Indeed, several of the 23 afterglow candidates in the RASS sample of Greiner et al. (2000) showed power-law-like light curves (constructed similarly to the anticipated eROSITA data, namely there were several 10–30 s exposures separated by 1.5-hour intervals) but proved to be associated with stars.

Stellar flares demonstrate a remarkable variety of properties such as the duration and shape of the rising and decaying phases, the peak flux and its ratio to the quiescent level. Unfortunately, virtually all studies of these properties reported in the literature are strongly affected by the detection efficiency and strategy of the particular surveys (see Favata & Micela 2003; Güdel 2004 for review). Therefore, it is difficult to make even crude estimates of the frequency of stellar flares resembling GRB afterglows in eROSITA observations. Nevertheless, we may mention a couple of aspects that may help distinguish stellar episodes from afterglows. First, there is a well-known tendency for stonger flares to occur in stellar coronae with stronger quiescent X-ray activity (Favata & Micela 2003; Güdel 2004)). Therefore, a flare exceeding our proposed threshold for GRB afterglows,  $\sim 2 \times 10^{-13}$  erg s $^{-1}$  cm $^{-2}$  (0.5–2 keV), should typically be associated with a star that will be seen as a persistent source (with  $F_X \gtrsim 5 \times 10^{-14}$  erg s $^{-1}$  cm $^{-2}$ , 0.5–2 keV) in repeated eROSITA all-sky scans. Secondly, typical stellar flares have spectra that are typically significantly softer (Favata & Micela 2003) than those of GRB afterglows. Although our afterglow detection limit is relatively low ( $\sim 9$  counts during the third flux measurement), the total number of photons accumulated during the  $f_1$  measurement will typically be  $\sim 10^2$  in the 0.5–2 keV energy band, so that there will be a sufficient number of photons detected above 2 keV to discriminate the hard spectrum of an afterglow from the softer spectrum of a stellar flare. Additional valuable information above 6 keV can be provided by the ART-XC telescope if an afterglow falls into its

(smaller relative to eROSITA) FoV. Finally, as we discuss below, multi-wavelength information should be very helpful.

### 4.3 Cross-correlation with optical and infrared catalogues

The anticipated availability by the time of the *SRG* mission of a number of sensitive optical and infrared photometric surveys covering the whole sky or its large fractions should greatly help in distinguishing coronally active stars and AGN from host galaxies of GRB afterglows. Indeed, the non-flaring X-ray to optical flux ratio,  $F_X/F_{\text{opt}}$ , never exceeds  $\sim 10^{-3}$ , for stellar coronae (e.g. Güdel 2004), and only during the most extreme flares can the coronal X-ray luminosity become comparable to the bolometric luminosity of the star (see Osten et al. 2010 and references therein; also Uzawa et al. 2011). Therefore, if a stellar flare satisfies our GRB afterglow detection criterion (Task 1) and hence have a peak flux  $F_X \sim 10^{-12} \text{ erg s}^{-1} \text{ cm}^{-2}$  (0.5–2 keV), it should be readily associated with a relatively bright star of  $R \lesssim 20$  in the Sloan Digital Sky Survey (SDSS, which has imaged  $\approx 1/3$  of the sky in the  $u$ ,  $g$ ,  $r$ ,  $i$  and  $z$  bands with a typical sensitivity of  $R = 22.2$ , Data Release 8, Aihara et al. 2011) and/or in the  $3\pi$  Steradian Survey of the the Panoramic Survey Telescope and Rapid Response System (Pan-STARRS, which is planned to image  $3/4$  of the sky in the  $g$ ,  $r$ ,  $i$ ,  $z$  and  $y$  filters down to  $R = 24$ , Kaiser & Pan-STARRS Team 2002). Indeed, the number density of  $R < 20$  stars at high Galactic latitudes is less than 1 per square minute (e.g. Jurić et al. 2008), whereas the eROSITA localisation accuracy is better than 10 arcsec.

As concerns AGN, based on the results of a number of previous extragalactic X-ray surveys (e.g. Aird et al. 2010) it can be expected that the optical to X-ray flux ratio will be in the range  $0.1 < F_X/F_{\text{opt}} < 10$  for the majority of AGN detected by eROSITA. Consequently, relatively bright AGN with  $F_X \gtrsim 10^{-13} \text{ erg s}^{-1} \text{ cm}^{-2}$  (0.5–2 keV), i.e. such AGN that may produce flares resembling GRB afterglows, should be associated with relatively bright,  $R \sim 19 \pm 2$ , objects in the SDSS and PanSTARRS catalogues. Furthermore, it is expected (Sazonov et al., in preparation) that the absolute majority of such moderately X-ray bright AGN should be readily identifiable with the help of the recently published all-sky catalogue of mid-infrared sources detected by the *Wide-Field Infrared Survey Explorer* (*WISE*, Lake et al. 2012).

In comparison, the host galaxies of typical GRBs observed so far are generally faint, with about half being weaker than  $R_{\text{ab}} = 23.5$  and  $K_{\text{ab}} = 22.5$  (Savaglio, Glazebrook & Le Borgne 2009). Since, there is no significant dependence of GRB fluence on redshift (Sakamoto et al. 2011), the host galaxies of GRBs associated with eROSITA afterglows, will typically be as dim. We conclude that the absence of a bright counterpart in the publicly available catalogues of large-area optical and infrared photometric surveys will be a strong additional signature in favour of a GRB afterglow origin of transients showing a power-law-like decline.

**Table 2.** Expected detection rates for afterglows associated with various types of GRBs

Type	$N_1 (F_e = 2 \times 10^{-13} \frac{\text{erg}}{\text{s cm}^2})$ , per year
Long GRBs	6.8 – 7.6
Short GRBs	$\sim 0.1$
GeV GRBs	$< 1.5$
XRFs	$\sim 0.4$

## 5 AFTERGLOWS FROM OTHER CLASSES OF GRBS

Some uncertainty in the number of afterglows that can be detected with eROSITA arises from the lack of information about the low-fluence end of the  $\log N$ — $\log S$  distribution of long GRBs. In addition, we should take into account the possibility of detecting afterglows associated with some additional subclasses of GRBs.

### 5.1 Short GRBs

In comparison to long GRBs (LGRB), short GRBs (SGRB) are rarer and fainter. Indeed, about 10 long bursts are localised by *Swift* for every short burst, and the average fluence of SGRBs is an order of magnitude lower than that of LGRBs. The X-ray afterglows of SGRBs are also faint, which might point at different properties of the progenitor and circumburst environment. However, using a large sample of 37 short and 421 long GRBs, Nysewander, Fruchter & Pe'er (2009) found that SGRBs follow approximately the same correlation between X-ray afterglow brightness and prompt  $\gamma$ -ray fluence as do LGRBs. This suggests that the eROSITA detection rate of SGRB afterglows should be relatively low. Adopting  $F_e = 2 \times 10^{-13} \text{ erg s}^{-1} \text{ cm}^{-2}$  as the detection limit for Task 1, we find that only 7 of 27 SGRBs with X-ray afterglow flux measurements in the sample of Nysewander, Fruchter & Pe'er (2009) have  $\tau_m > 0$ , i.e.  $\tau_e > 8$  hr, implying that the corresponding detection rate  $N_1$  of SGRB afterglows will be  $\approx 40$  times lower than for LGRB afterglows (since almost all LGRB afterglows in the *Swift* sample have  $\tau_e > 8$  hr). Thus, taking into account our estimates for long bursts (Table 1), SGRB afterglows will only rarely,  $\sim 0.1$  per year (see Table 2), satisfy the eROSITA detection criterion for non-triggered GRBs.

### 5.2 Ultra hard (GeV) GRBs

The energy range of *Swift*/BAT is narrow (15–150 keV) with respect to the observed variety of GRB prompt emission spectra (Virgili et al. 2011). The effective energy range of *CGRO*/BATSE for GRB detection was similar, 50–300 keV. This suggest that there might exist a population of GRBs with ultra-hard prompt emission and moderate or undetectable signal in the hard X-ray band. This hypothesis can now be tested with the Large Area Telescope (LAT) on board *Fermi*, which is sensitive from 30 MeV to 100 GeV and has a FoV of  $\approx 2.4$  sr (Atwood et al. 2009). The detection rate of *Fermi*/LAT is  $\approx 10$  bursts per year, which corresponds to  $R \approx 50$  bursts per year over the whole sky. All of

the long GRBs detected by LAT so far occurred outside the BAT FoV. Detailed analysis of prompt and afterglow emission properties of the LAT-detected GRBs (Racusin et al. 2011; Cenko et al. 2011) indicates that although these GRBs have the largest fluences ever observed, their afterglows still fall within the flux distribution of *Swift*/BAT-triggered GRBs, exactly near its upper boundary, whereas the spectral and temporal behaviour of the LAT-triggered GRB afterglows are quite similar to those of the BAT-triggered ones.

Because the scatter in the X-ray afterglow fluxes of LAT-triggered GRBs is fairly small (probably owing to the fairly poor statistics provided by less than 10 GRBs in the current sample), some instructive estimates can be obtained assuming that all of these afterglows have some 'average' form. Using the data from Swenson et al. (2010), we find that a typical LAT-triggered GRB afterglow has  $F_{X,12} \sim 2 \times 10^{-12} \text{ erg s}^{-1} \text{ cm}^{-2}$  (0.5–2 keV flux at 12 hours after the prompt emission) and  $\alpha \approx 1.5$  (temporal decay index). Thus, assuming an eROSITA detection limit per scan of  $F_e = 2 \times 10^{-13} \text{ erg s}^{-1} \text{ cm}^{-2}$ , such afterglows can be detected by eROSITA up to  $\tau_e \approx 57$  hours after the prompt emission (see Sect. 2.1). Hence, the corresponding detection rate  $N_1 \approx 0.66$  per year over the whole sky (given a total rate of  $R = 50$  of such bursts per year). In addition, there might be faint ultra-hard GRBs remaining below the LAT detection limit but capable of producing X-ray afterglows detectable by eROSITA for more than 8 hours. However, by analogy with classical GRBs (see Table 1), the number of such afterglows is unlikely to exceed the number of afterglows associated with detectable ultra-hard GRBs. We thus expect the total eROSITA detection rate of afterglows of ultra-hard GRBs to be less than 1.5 per year (see Table 2).

### 5.3 X-ray Flashes

There can also be X-ray afterglows associated with so-called 'X-ray flashes', originally burst-like (shorter than 1000 s) events detected in X-rays by the Wide Field Camera on *BeppoSAX* but not detected by the Gamma-Ray Monitor on the same satellite (Heise et al. 2001). Comprehensive studies based on data from *BeppoSAX* (Kippen et al. 2003), *HETE-2* (Sakamoto et al. 2005) and most recently *Swift* (Sakamoto et al. 2008) have not found significant differences between the duration and sky distributions of XRFs and 'classical' GRBs. Moreover, the spectral properties of XRF prompt emission were found to be similar to those of GRBs, except that the peak energies  $E_{peak}^{obs}$  (of the prompt  $\nu F_\nu$  spectrum), peak fluxes  $F_{peak}$  and fluences  $S_E$  of XRFs are much smaller. This suggests that X-ray flashes arise from the same phenomenon as GRBs, continuing the GRB population to low  $E_{peak}$  (Sakamoto et al. 2008).

The Wide-Field X-ray Monitor on board *HETE-2* makes it possible to readily estimate the rate of observable XRFs in comparison with GRBs, because its threshold for detection and localisation of bursts in terms of the peak photon number flux is only weakly dependent on  $E_{peak}^{obs}$ , i.e. nearly the same for XRFs and GRBs (Sakamoto et al. 2005). Based on the fluence ratio  $S_X(2-30 \text{ keV})/S_\gamma(30-400 \text{ keV})$ , out of a total of 45 bursts in the *HETE-2* sample there are 16 XRF, nearly half of which have  $E_{peak}^{obs} < 20 \text{ keV}$  and a peak flux of  $< 0.2 \text{ ph s}^{-1} \text{ cm}^2$  in the 50–300 keV energy band. Here we are interested in such events because i)

they seem to be missing from the  $\log N$ – $\log S$  distribution of BATSE GRBs (see figures 16 and 17 in Sakamoto et al. 2005), and ii) detection of such bursts by *Swift*/BAT in its 15–150 keV energy range is challenging. Studies of XRF afterglow emission based on *BeppoSAX* and *HETE-2* (D'Alessio et al. 2006) and on *Swift* (Sakamoto et al. 2008) samples have produced somewhat controversial results. In particular, D'Alessio et al. (2006) found that XRF afterglow light curves are similar to those of classical GRBs, including the break feature at late times (Panaitescu 2007). The XRF afterglow fluxes were also found to be not much lower than for GRB afterglows. On the other hand, the afterglows of XRFs from the more extensive *Swift*/XRT sample, consisting of bursts with  $E_{peak}^{obs} > 20 \text{ keV}$ , exhibit no break in the light curves and are weaker by a factor of 2 or more compared to that of classical GRBs (Sakamoto et al. 2008). To extend this result to XRFs with  $E_{peak}^{obs} < 20 \text{ keV}$ , we may assume that there is a positive correlation between prompt emission fluence and X-ray afterglow flux, i.e. the afterglows of such XRF should be fainter than those of XRFs with  $E_{peak}^{obs} > 20 \text{ keV}$ . Putting all these facts together, we estimate that afterglows of XRFs with  $E_{peak}^{obs} < 20 \text{ keV}$  are approximately 4 times rarer and at least 2 times fainter than afterglows of typical *Swift* bursts. Therefore, the total detection rate of the former is expected at the level  $\sim 0.4$  per year (see Table 2).

## 6 'ORPHAN' AFTERGLOWS AND FAILED GRBS

Even after considering various subclasses of GRBs and XRFs, our account of afterglows that can be detected by eROSITA is still incomplete. An additional contribution may come from afterglows that are not preceded by prompt  $\gamma$ - or X-ray emission, which are often referred to as 'orphan afterglows' (OA). The standard theory of GRBs, dealing with strongly beamed emission of a highly relativistic (initial Lorentz factor  $\Gamma \sim 100 - 1000$ ) jet, allows for the existence of three classes of OA: 1) on-axis afterglows, observed within the opening angle of the initial relativistic jet but outside its narrow  $\gamma$ -ray emitting (due to a larger Lorentz factor) component; 2) off-axis afterglows, observed outside the initial jet after the jet break time, when the jet expands sideways (Nakar & Piran 2003); and 3) afterglows of so-called 'failed GRBs' (FGRB), associated with baryon-contaminated fireballs with an initial Lorentz factor of much less than 100 but still greater than unity (Huang, Dai & Lu 2002).

The light curve of an off-axis OA should initially rise until a moment that approximately corresponds to the jet-break time of 'normal' GRB afterglows ( $10^4 - 10^5 \text{ s}$ , Panaitescu 2007) and then decay in the usual post-jet-break manner (with a decay slope greater than 1.5 and typically near 2.0, see Nakar & Piran 2003). Hence, for such an afterglow to satisfy our Task 1 identification criteria (i.e. a power-law-like decay), the required three successive (spanning 8 hours) detections by eROSITA should take place after the moment of maximal flux. However, the X-ray flux at this stage will typically be already too low for detection. Therefore, such off-axis events are unlikely to be found in significant numbers by eROSITA. As regards on-axis OAs, (Nakar & Piran 2003) summarised observational constraints



provided by the numbers of X-ray transients and GRBs detected by *Ariel 5*, *HEAO-1*, *ROSAT* and *BeppoSAX* and concluded that the average ratio of the opening angle of GRB jets to that of their  $\gamma$ -ray emitting components is  $\lesssim 2$ . This suggests that eROSITA may find a comparable number of orphan afterglows to that of 'normal' afterglows, i.e. several events per year (see Table 1) and can thereby improve the constraints on the structure of relativistic jets in GRBs.

As concerns failed GRBs, their existence seems rather natural from a theoretical point of view, because it is hard to produce a pure (in terms of the baryonic content) highly relativistic flow. The collapsar model (MacFadyen & Woosley 1999) predicts a great variety in the baryon mass and released energy, and consequently in the initial Lorentz factor  $\Gamma$  of the produced fireball, among different events. In most cases,  $\Gamma$  is expected to be low ( $\ll 100$ ), leading to FGRBs that have almost the same initial energy as normal GRB fireballs ( $10^{51} - 10^{53}$  erg) but are polluted by baryons with mass  $\sim 10^{-5} - 10^{-3} M_{\odot}$ . It has also been suggested that a large population of FGRBs could arise if the jet failed to break out of the progenitor star in the collapsar model (Bromberg et al. 2011). In such a case, a UV/soft X-ray thermal burst followed by an afterglow with some distinct features should be observed (Xu et al. 2012). It is practically impossible to predict the rate of such events, but eROSITA may shed light on this explored population.

## 7 SUMMARY AND DISCUSSION

The results of this study imply that it should be possible to detect and identify, by the shape of the light curve, 4–8 X-ray afterglows associated with classical long GRBs per year in the eROSITA all-sky survey data (see Table 1). The exact number will depend on the shape of the  $\log N$ – $\log S$  distribution of GRBs at low fluences (near the effective threshold of *CGRO/BATSE* and *Swift/BAT*). In addition, eROSITA is expected to find a small number of afterglows associated with other classes of GRBs such short bursts, GeV bursts and X-ray flashes (Table 2). Thus, by the end of the 4-year survey, a sample of at least 20–40 X-ray afterglows can be accumulated. This sample, although smaller than the already existing samples of afterglows, will nevertheless be interesting for systematic studies of GRBs and their afterglows because of its unbiased nature. In particular, it can be used to construct an unbiased distribution of X-ray afterglow fluxes and to obtain constraints on the shape of the  $\log N$ – $\log S$  distribution of GRBs.

The total number of afterglows detected by eROSITA may prove higher, perhaps by a factor of 2 or more, due to orphan afterglows and failed GRBs. The actual detection rate will thus provide interesting constraints on the properties of relativistic jets associated with the collapse of massive stars.

The proposed algorithm for searching afterglows of non-triggered GRBs (Task 1) in the eROSITA data is based on checking if the light curve of a given source resembles a power-law decline. Although such a procedure may erroneously identify a large number of other types of variable X-ray sources (e.g. AGN and stellar flares) as GRB afterglows, most of such contaminants should be easily revealed through cross-checking of successive eROSITA all-sky scans

and cross-correlation with large-area optical and infrared source catalogues.

We have also discussed the possibility of using the eROSITA data for searching for afterglows of triggered (by any GRB monitors) GRBs. Since the coordinates of the triggered bursts will be known, eROSITA just needs to detect a few photons from the afterglow in one  $\sim 40$  s scan. As a result, the total number of such events can be large,  $\sim 20 - 60$  per year depending on the  $\log N$ – $\log S$  function (see Table 1), provided that at the time of the *SRG* mission there are GRB monitors covering most of the sky at any given time. X-ray afterglows detected in this way can be interesting for statistical studies addressing the same scientific problems as discussed above in relation to the search for afterglows of non-triggered GRBs.

Finally, although *SRG* data transfer is planned to occur only once per day, accurate ( $\lesssim 30''$ ) coordinates provided by eROSITA within  $\sim 1$  day after the event on afterglows of GRBs and orphan afterglows can be valuable for scheduling further follow-up observations.

## APPENDIX 1: TASK 1 DETECTION LIMIT

Here we determine the eROSITA 0.5–2 keV detection limit  $F_e$  for candidate GRB afterglows. The question we need to answer is to what accuracy do we need to obtain three consecutive flux measurements,  $f_1$ ,  $f_2$  and  $f_3$ , to be able to conclude with certainty that the X-ray flux is decaying as a power law? Because the result is mostly sensitive to  $f_3$  (i.e. the latest flux measurement), the condition  $f_3 > F_e$  must be fulfilled.

To this end, we simulated light curves of GRB afterglows as would be measured by eROSITA, assuming that photon counts obey the Poisson distribution. The mathematical problem consists of fitting the intrinsic afterglow parameters  $F_{X,12}$ ,  $t_0$  and  $\delta$  (equation 1) given  $f_1$ ,  $f_2$  and  $f_3$  with their corresponding statistical uncertainties. In particular, the power-law slope can be derived analytically from equation (3). We found that, if the intrinsic slope  $\delta = 1.3$  and we require the measured value of  $\delta$  to lie in the range from  $\approx 0.5$  to  $\approx 3.5$  this conservatively broad range reflects the observed scatter in decay indices taking into account the post-break phase (Nysewander, Fruchter & Pe'er 2009)), then  $f_3$  should be measured with accuracy better than  $\sim 30\%$ , i.e. the latest measurement must be based on at least 9 photons. Figure 5 illustrates this conclusion. It shows the result of multiple realisations of a light curve for fixed intrinsic parameters:  $\delta = 1.3$ ,  $\tau_1 = 1$  hr (the time of the first flux measurement) and  $f_3$  corresponding to 9 photons. The resulting family of possible power-law solutions is bounded (within  $1\sigma$ ) by two curves that correspond to  $\delta \simeq 0.4$  and  $\delta \simeq 3.3$ . For a characteristic X-ray afterglow spectrum with a photon index  $\Gamma = 2$  and the preliminary eROSITA response matrix (<http://mpe.mpg.de/erosita/response/>), the 9 counts limit corresponds to  $F_e \simeq 2 \times 10^{-13}$  erg s $^{-1}$  cm $^{-2}$  for a diametral transition of a source through the eROSITA FoV.

In reality, the effective detection threshold might be somewhat higher than estimated above because there is some uncertainty in the afterglow spectral properties and characteristics of the eROSITA telescope. We estimate that

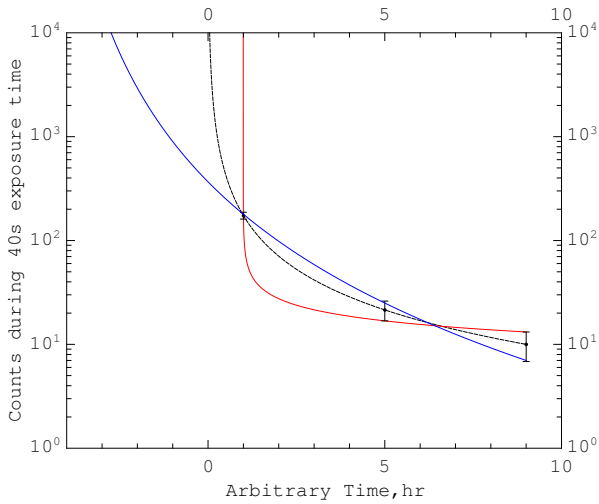


**Figure 5.** Uncertainty in the inferred power-law slope  $\delta$  of an afterglow light curve induced by the statistical (Poisson) uncertainties of count rates measured in 3 consecutive scans. The adopted intrinsic light curve is shown in black: its slope is  $\delta = 1.3$ , the first detection takes place at  $\tau_1 = 1$  hour after prompt emission ( $t = 0$  here) and the mean flux during the third measurement corresponds to 9 photons. For each of a large number of simulated data sets, the best-fitting power law was found. These solutions are distributed (within  $1\sigma$ ) around the intrinsic light curve from  $\delta \simeq 0.4$  (red curve) to  $\delta \simeq 3.3$  (blue curve).

$F_e \simeq 3 \times 10^{-13} \text{ erg s}^{-1} \text{ cm}^{-2}$  can be regarded as a conservative value.

## APPENDIX 2: TASK 2 DETECTION LIMIT

In the case of Task 2, the effective afterglow flux limit is mainly determined by the background level of the eROSITA detectors. It is expected that in the 0.5–2 keV energy band, the cosmic X-ray background (Galactic and extragalactic) will dominate over the particle background. After excluding bright extragalactic sources that will be detected as individual point sources, the total background count rate in the 0.5–2 keV energy band over the eROSITA FoV is expected to  $\approx 5$  counts per second (Prokopenko & Gilfanov 2009). This corresponds to  $\approx 0.012$  counts inside the region of half-power diameter (HPD,  $\approx 29''$ ) of the eROSITA point spread function over a 40 s exposure time. According to the Poisson distribution, the probability that 2 or more background photons will be detected by chance in the HPD region is  $\approx 7.4 \times 10^{-5}$ . Assuming that the position of a given GRB is known to an accuracy of  $\sim 10'$  (as is e.g. the case for GRBs detected by *Swift*/BAT), the probability of finding 2 or more background events inside this localisation region is less than  $3 \times 10^{-2}$ , which, however, will not provide  $3\sigma$  confidence of source detection. Therefore, it is reasonable to demand at least 3 counts as the detection limit for Task 2. This corresponds to a flux limit of  $F_d \approx 7 \times 10^{-14} \text{ erg s}^{-1} \text{ cm}^{-2}$  (0.5–2 keV). However, such a detection will provide poor information about the afterglow brightness. To allow the accuracy of flux measurement of at least  $\sim 50\%$  and account for some remaining uncertainty in the eROSITA background level, we adopt a more

conservative value  $F_d = 1 \times 10^{-13} \text{ erg s}^{-1} \text{ cm}^{-2}$ , which approximately corresponding to 4 counts from a point source in the localisation region.

## ACKNOWLEDGEMENTS

The research made use of grants RFBR 11-02-12271-ofi-m and NSH-5603.2012.2, and programme P-21 of the Russian Academy of Sciences. IK acknowledges the support of the Dynasty Foundation.

## REFERENCES

- Aihara H., et al., 2011, *ApJS*, 193, 29  
Aird J., et al., 2010, *MNRAS*, 401, 2531  
Atwood, W. B., Abdo, A. A., Ackermann, M., et al. 2009, *ApJ*, 697, 1071  
Berger, E., Kulkarni, S. R., Fox, D. B., et al. 2005, *ApJ*, 634, 501  
Bromberg O., Nakar E., Piran T., Sari R., 2012, *ApJ*, 749, 110  
Campana S., et al., 2012, *MNRAS*, 421, 1697  
Cenko, S. B., Frail, D. A., Harrison, F. A., et al. 2011, *ApJ*, 732, 29  
Dai, X. 2009, *ApJ*, 697, L68  
D’Alessio, V., Piro, L., & Rossi, E. M. 2006, *A&A*, 460, 653  
de Pasquale, M., Piro, L., Gendre, B., et al. 2006, *AAP*, 455, 813  
Favata, F., Micela, G. 2003, *SSRv*, 108, 577  
Gehrels, N., Barthelmy, S. D., Burrows, D. N., et al. 2008, *ApJ*, 689, 1161  
Gehrels N., Ramirez-Ruiz E., Fox D. B., 2009, *ARA&A*, 47, 567  
Greiner J., Hartmann D. H., Voges W., Boller T., Schwarz R., Zharikov S. V., 2000, *A&A*, 353, 998  
Güdel, M. 2004, *A&ARv*, 12, 71  
Heise, J., Zand, J. I., Kippen, R. M., Woods, P. M. 2001, *Gamma-Ray Bursts in the Afterglow Era Proceedings of the International Workshop Held in Rome, Italy, 17-20 October 2000*, p. 16, Costa E., Frontera F., Hjorth J. (Eds.), Springer-Verlag Berlin Heidelberg New York  
Huang, Y. F., Dai, Z. G., Lu, T. 2002, *MNRAS*, 332, 735  
Hurley K., et al., 2011, *AIPC*, 1358, 385  
Jurić M., et al., 2008, *ApJ*, 673, 864  
Kaiser N., et al., 2002, *SPIE*, 4836, 154  
Kippen R. M., Woods P. M., Heise J., in’t Zand J. J. M., Briggs M. S., Preece R. D., 2003, *AIPC*, 662, 244  
Kulkarni S. R., et al., 1998, *Natur*, 395, 663  
Lake S. E., Wright E. L., Petty S., Assef R. J., Jarrett T. H., Stanford S. A., Stern D., Tsai C.-W., 2012, *AJ*, 143, 7  
Liang E., Zhang B., Virgili F., Dai Z. G., 2007, *ApJ*, 662, 1111  
MacFadyen, A. I., Woosley, S. E. 1999, *ApJ*, 524, 262  
McHardy I. M., Papadakis I. E., Uttley P., Page M. J., Mason K. O., 2004, *MNRAS*, 348, 783  
McHardy I., 2010, *LNP*, 794, 203, T. Belloni (Ed.), *The Jet Paradigm: From Microquasars to quasars ,X-Ray Vari-*

- ability of AGN and Relationship to Galactic Black Hole Binary Systems, Springer, Berlin Heidelberg
- Nakar, E., Piran, T. 2003, *NewA.*, 8, 141
- Nousek, J. A., Kouveliotou, C., Grupe, D., et al. 2006, *ApJ*, 642, 389
- Nysewander, M., Fruchter, A. S., Pe'er, A. 2009, *ApJ*, 701, 824
- Osten R. A., et al., 2010, *ApJ*, 721, 785
- Panaitescu, A. 2007, *MNRAS*, 380, 374
- Pavlinisky M., et al., 2011, *SPIE Proc.*, 8147, 5
- Pavlinisky M., et al., 2012, *SPIE Proc.*, in press
- Pian E., et al., 2006, *Nature*, 442, 1011
- Porciani C., Madau P., 2001, *ApJ*, 548, 522
- Predehl P., et al., 2011, *SPIE*, 8145, 247
- Prokopenko, I. G., Gilfanov, M. R. 2009, *Astronomy Letters*, 35, 294
- Racusin, J. L., Oates, S. R., Schady, P., et al. 2011, *ApJ*, 738, 138
- Rossi E., Lazzati D., Rees M. J., 2002, *MNRAS*, 332, 945
- Sakamoto, T., Lamb, D. Q., Kawai, N., et al. 2005, *ApJ*, 629, 311
- Sakamoto, T., Hullinger, D., Sato, G., et al. 2008, *ApJ*, 679, 570
- Sakamoto, T., Barthelmy, S. D., Barbier, L., et al. 2008, *ApJS*, 175, 179
- Sakamoto, T., Barthelmy, S. D., Baumgartner, W. H., et al. 2011, *ApJS.*, 195, 2
- Savaglio, S., Glazebrook, K., Le Borgne, D. 2009, *ApJ*, 691, 182
- Sazonov, S. Y., Lutovinov, A. A., Sunyaev, R. A. 2004, *Nature*, 430, 646
- Soderberg A. M., et al., 2004, *Natur*, 430, 648
- Stern, B. E., Tikhomirova, Y., Kompaneets, D., Svensson, R., & Poutanen, J. 2001, *ApJ*, 563, 80
- Stern, B. E., Tikhomirova, Y., Svensson, R. 2002, *ApJ*, 573, 75
- Swenson, C. A., Maxham, A., Roming, P. W. A., et al. 2010, *ApJ*, 718, L14
- Timmer, J., Koenig, M. 1995, *A&A*, 300, 707
- Uzawa A., et al., 2011, *PASJ*, 63, 713
- Virgili F. J., Qin Y., Zhang B., Liang E., 2012, *MNRAS*, 424, 2821
- Xu M., Nagataki S., Huang Y. F., Lee S.-H., 2012, *ApJ*, 746, 49
- Zhang B., Fan Y. Z., Dyks J., Kobayashi S., Mészáros P., Burrows D. N., Nousek J. A., Gehrels N., 2006, *ApJ*, 642, 354